

Direct Observation of Topological Phonons in Graphene

Jiade Li,^{1,4} Jiangxu Li,² Jilin Tang,^{3,5} Zhiyu Tao,^{1,4} Siwei Xue,¹ Jiayi Liu,² Hailin Peng,^{3,5,*}

Xing-Qiu Chen^{2,†}, Jiandong Guo^{1,4,6,‡} and Xuetao Zhu^{1,4,6,§}

¹*Beijing National Laboratory for Condensed Matter Physics and Institute of Physics, Chinese Academy of Sciences, Beijing 100190, China*

²*Shenyang National Laboratory for Materials Science, Institute of Metal Research, Chinese Academy of Sciences, Shenyang 110016, China*

³*Center for Nanochemistry, Beijing Science and Engineering Center for Nanocarbons, Beijing National Laboratory for Molecular Sciences, College of Chemistry and Molecular Engineering, Peking University, Beijing 100871, China*

⁴*School of Physical Sciences, University of Chinese Academy of Sciences, Beijing 100049, China*

⁵*Beijing Graphene Institute (BGI), Beijing 100095, China*

⁶*Songshan Lake Materials Laboratory, Dongguan, Guangdong 523808, China*



(Received 22 March 2023; accepted 28 July 2023; published 14 September 2023)

Phonons, as the most fundamental emergent bosons in condensed matter systems, play an essential role in the thermal, mechanical, and electronic properties of crystalline materials. Recently, the concept of topology has been introduced to phonon systems, and the nontrivial topological states also exist in phonons due to the constraint by the crystal symmetry of the space group. Although the classification of various topological phonons has been enriched theoretically, experimental studies were limited to several three-dimensional (3D) single crystals with inelastic x-ray or neutron scatterings. The experimental evidence of topological phonons in two-dimensional (2D) materials is absent. Here, using high-resolution electron energy loss spectroscopy following our theoretical predictions, we directly map out the phonon spectra of the atomically thin graphene in the entire 2D Brillouin zone, and observe two nodal-ring phonons and four Dirac phonons. The closed loops of nodal-ring phonons and the conical structure of Dirac phonons in 2D momentum space are clearly revealed by our measurements, in nice agreement with our theoretical calculations. The ability of 3D mapping (2D momentum space and energy space) of phonon spectra opens up a new avenue to the systematic identification of the topological phononic states. Our work lays a solid foundation for potential applications of topological phonons in superconductivity, dynamic instability, and phonon diode.

DOI: [10.1103/PhysRevLett.131.116602](https://doi.org/10.1103/PhysRevLett.131.116602)

Topological phononics, including the acoustic waves in artificial metamaterials and the phonons in solid crystalline materials, have been attracting extensive attention. Although the progress of topological acoustic artificial metamaterials [1–6] are highly exciting, topological phonons (TPs) in solid crystalline materials are of fundamental importance. Analogous to the topological classifications in electronic systems, TPs in solid crystalline materials have been theoretically classified into Weyl phonons [7–9], Dirac phonons [10], nodal-line (ring) phonons [11,12], and hourglass phonons [13]. Naturally, TPs produce nontrivial topologically protected surface or edge states, which are able to conduct phonons without scattering. This results in low-dissipation transmission and, thus, carries very promising properties and rich application perspectives [14]. Conceptually, phonons are effective in the whole region of the frequency without the limits of Fermi energy and the Pauli exclusive principle and, thus, the topological phenomena of phonons should be richer than topological electrons for a solid material.

Unlike the fast responses of topological electrons to external electric or magnetic fields, the signature of TPs is hard to be captured by measuring macroscopic properties. Hence, the characterization of TPs relies on the measurement of phonon spectra, analogous to the determination of electronic topology by mapping electronic band structures. However, to characterize the energetic difference between topological phononic bands, usually in the range from ~ 0.1 to ~ 10 meV, requires high-resolution experimental techniques, which are typically more difficult than elucidating those between topological electronic bands in the scale of ~ 100 to ~ 1000 meV. In addition, to obtain the global topological phononic feature, accurate and efficient measurements of the phonon spectra in the entire momentum space are needed. This brings big challenges to the current mainstream phonon measurement techniques, such as inelastic x-ray or neutron scattering upon the preparation of high-quality single crystalline samples. Known measurements of TPs [7,15–17] were only limited to observing the crossovers of some bulk phonon branches along a

specific momentum direction, lacking a global characterization of the phononic topology. Although TPs also have been predicted in a series of two-dimensional (2D) materials [18–20], it is almost impossible for x-ray or neutron scattering techniques to detect phonons of 2D materials because they are insensitive to the surfaces or monolayer materials. Hence, no experimental verification of TPs in 2D materials has been available to date. Apparently, there is an urge to confirm the experimental evidence for 2D TPs.

In this context, the electron beam in use for the high-resolution electron energy loss spectroscopy (HREELS) with a reflective measuring geometry provides the penetration length most suitable for surfaces (generally, several atomic layers) or 2D materials. Hence, the HREELS would be the suitable tool to measure topologically protected phononic surface states and, in particular, it is the most appropriate one to characterize TPs of 2D materials. More importantly, the recently developed 2D HREELS technique [21,22] enables the efficient mapping of phonon dispersions, with high resolutions of both energy and momentum, within the entire momentum space. These advantages provide the key prerequisite to depict the global topology of phonons for 2D materials.

Interestingly, the ideal 2D single-atom-thick material, graphene, was recently predicted to host robust TPs including nodal-ring phonons (NPs) and Dirac phonons (DPs) [18]. Despite the phonon spectrum of graphene being extensively studied experimentally, all measurements were made along several typical high-symmetry paths [23,24]. Yet, mapping of the full phonon spectra of graphene throughout its entire 2D Brillouin zone (BZ) and the whole energy scale, the key to characterizing the global phononic topology, is still lacking. Given the fact that the traditional, but state-of-the-art HREELS technique seems to be feasible, this inspires us to explore the experimental verification of TPs of 2D materials using graphene as a benchmark. Here, we report the direct observation of 2D TPs, including both the NPs and DPs from the global phonon mapping of graphene by 2D HREELS.

Topological phonons of graphene.—Within a periodic crystal, the topological characteristics are mostly determined by symmetries. Generally, the classes of TPs of the 2D hexagonal lattice, which is isostructural to that of graphene, are highly rich. As illustrated in Fig. 1, its lattice possesses inversion (P), time-reversal (T), and out-of-plane mirror (M_z) symmetries. Following these symmetries, the crossings between phononic bands can be generally classified into DPs or NPs. DPs are protected by the P and T symmetries (i.e., the PT symmetry) and are characterized by Berry phases of $\pm\pi$ at the locations of Dirac points. The NPs are protected by the PT and M_z symmetries, featured by Berry phases of $\pm\pi$ in the inner region of the nodal rings. Upon the tilted degree of the phononic bands with respect to the $q_x - q_y$ momentum plane, type-I, type-II, and type-III DPs or NPs can be further classified

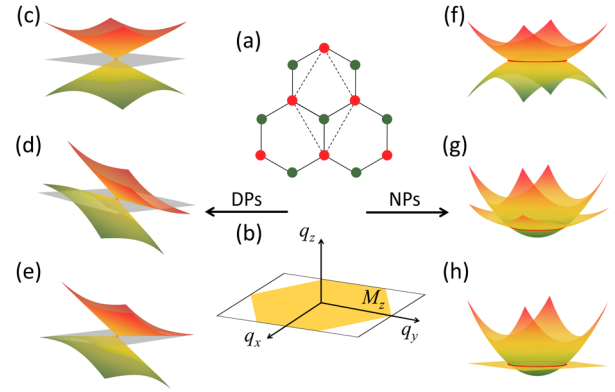


FIG. 1. Symmetries and classification of TPs in a 2D hexagonal lattice. (a),(b) 2D crystal structure and BZ of the hexagonal lattice, respectively. (c)–(e) Illustrations of type-I, type-II, and type-III DPs, respectively. (f)–(h) Illustrations of type-I, type-II, and type-III NPs, respectively.

[Figs. 1(c)–1(h)]. In order to capture this modeling analysis, we have performed the first-principles phonon calculations [Fig. 2(a)] and corresponding Berry phase calculations [details in the Supplemental Material (SM) [25]] of graphene, which agree well with our previous study [18]. Six TPs have been predicted, two of which are topological NPs and the other four of which are topological DPs. Among the four DPs, two type-I DPs (DP1 and DP2) occur at the K point and two type-II DPs (DP3 and DP4) form along the Γ - M and Γ - K paths, respectively [Fig. 2(a)]. DP1 describes the linear crossing of the phononic bands between the out-of-plane optical (ZO) and the acoustic (ZA) branches, whereas DP2 describes the linear crossing between the longitudinal optical (LO) and the acoustic

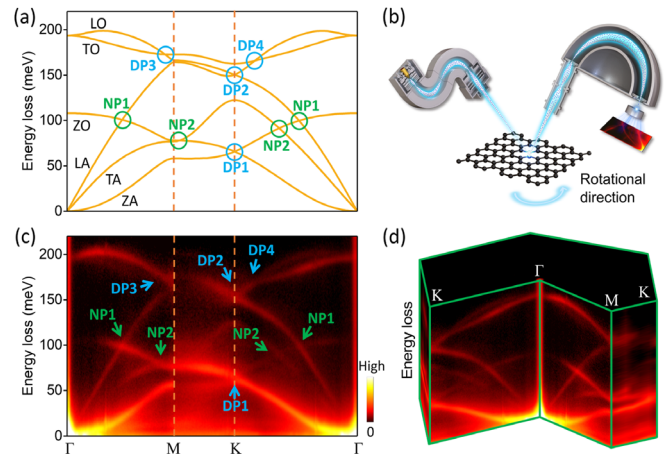


FIG. 2. Graphene phonon spectra and experimental setup. (a) Calculated graphene phonon spectra along the high-symmetry paths. (b) A schematic of the experimental setup. (c) Experimental graphene phonon spectra corresponding to (a). (d) 3D HREELS mapping of the graphene phonon spectra. The topological NPs and DPs are indicated by the green and blue circles (a) or arrows (c), respectively.

(LA) branches. DP3 and DP4 are the results of the linear crossings of the phononic bands between the LO and the transverse optical (TO) branches. In addition, two NPs, namely, NP1 and NP2, are formed from the continuously linear crossings of the phononic bands between the LA and ZO branches and between the transverse acoustic (TA) and ZO branches, respectively.

HREELS mapping of graphene phonons.—To experimentally identify the topological characteristics of the TPs, we have performed the HREELS measurements of the monolayer graphene samples, grown on the Cu(111)/sapphire substrate via chemical vapor deposition (details in the SM [25]). The 2D mapping was achieved by a specially designed lens system in combination with an electron monochromator and a hemispherical electron energy analyzer [Fig. 2(b)]. With such designs, the ultimate energy and momentum resolutions are better than 0.7 meV and 0.002 \AA^{-1} , respectively [21]. In this study, all the measurements were performed using an incident beam energy of 110 eV and an incident angle of 60° at room temperature. To compromise with the detection efficiency, we have set the resolutions to 3.8 meV and 0.03 \AA^{-1} for energy and momentum, respectively (Fig. S4 in the SM [25]), which enables the characterization of the TPs from the phonon spectra of graphene. Remarkably, the experimental mapping reproduced well the calculated phonon spectra. As a benchmark, it can be seen that along the high-symmetry Γ - M - K - Γ paths the experimentally measured spectra [Fig. 2(c)] perfectly agree with the theoretical ones [Fig. 2(a)]. The phononic band crossings, which are crucial for characterizing TPs, can be clearly visualized, as explicitly exhibited by the corresponding energy distribution

curve (EDC) stacks in Fig. S5 in the SM [25]. There is no doubt that the DPs and the nodal points on the NPs along the high-symmetry paths are reproduced by our experimental data. However, the global characterization of TPs, especially for the structural features of the whole NPs, has to be established by mapping phonons within the entire 2D BZ. In this sense, the mapping of the phonon spectra throughout the 2D momentum space (q_x, q_y) and energy space ($\hbar\omega$) is essential. Fortunately, in our current experimental setup for 2D HREELS, the high-resolution three-dimensional (3D) mapping ($q_x, q_y, \hbar\omega$) of the phonon spectra can be obtained by rotating the samples along the normal direction and collecting the 2D $\hbar\omega$ - q mapping with different azimuthal angles. As illustrated in Fig. 2(d), the 3D HREELS mapping of the graphene phonon spectra is compiled within the entire 2D BZ, which gives us the chance to study the structural features of graphene TPs.

Visualization of nodal-ring phonons.—As shown in Fig. 3, the structural features of graphene NPs are unambiguously revealed by the 3D mapping of the graphene phonon spectra. Although along the high-symmetry paths in Figs. 2(a) and 2(c) the crossings between both LA and ZO modes form the nodal points, these two nodal points are not isolated ones but form a closed loop due to the continuous phonon band crossings, as evidenced in Fig. 3(a) (marked by a bright cyan curve). Notably, the NP1 is flat, with a dispersionless feature at the energy of ~ 99 meV throughout the 2D BZ. The calculated spectrum in Fig. 3(c) indicates an excellent agreement that the LA and ZO modes result in the NP1 occurrence with a calculated energy of ~ 99.3 meV. Furthermore, we plot the experimental and calculated distributions of the energy

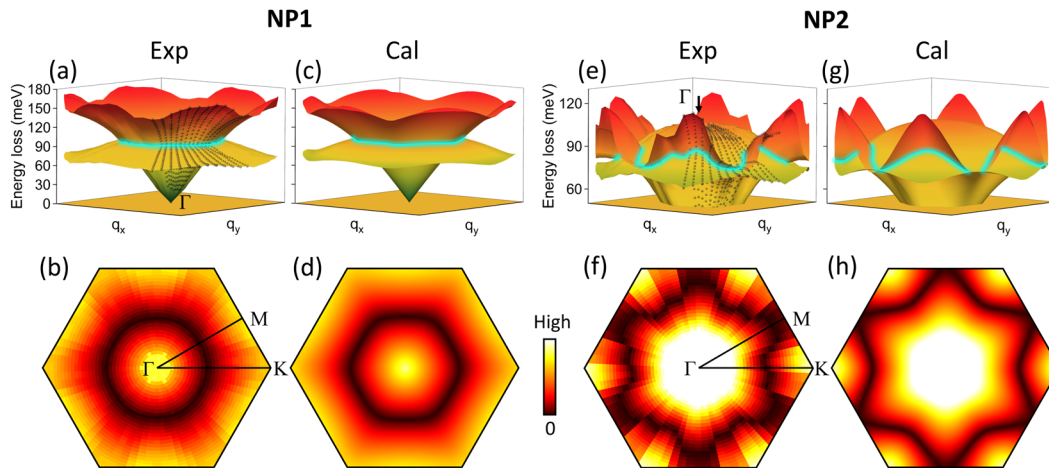


FIG. 3. Nodal-ring phonons of graphene. (a) Experimental observation of NP1 from the dispersion of LA and ZO branches in the 2D BZ from HREELS. The experimental data are marked by the black dots and the colored dispersions are reconstructed via linear interpolation from the experimental data. The data were taken by varying the azimuthal angle by 5° from the Γ - K direction each time until a total rotation of 60° (to the nearest Γ - K direction) is acquired. The entire spectrum is obtained by duplicating the experimental data according to the sixfold symmetry. (b) Projected shape of NP1 obtained from the measured energy gap between the LA and ZO branches in the first BZ. (c), (d) The calculated results corresponding to (a) and (b), respectively. (e)–(h) The corresponding results for NP2 from the experiments and calculations of the TA and ZO branches. The NPs are highlighted by bright cyan lines in (a), (c), (e), and (g).

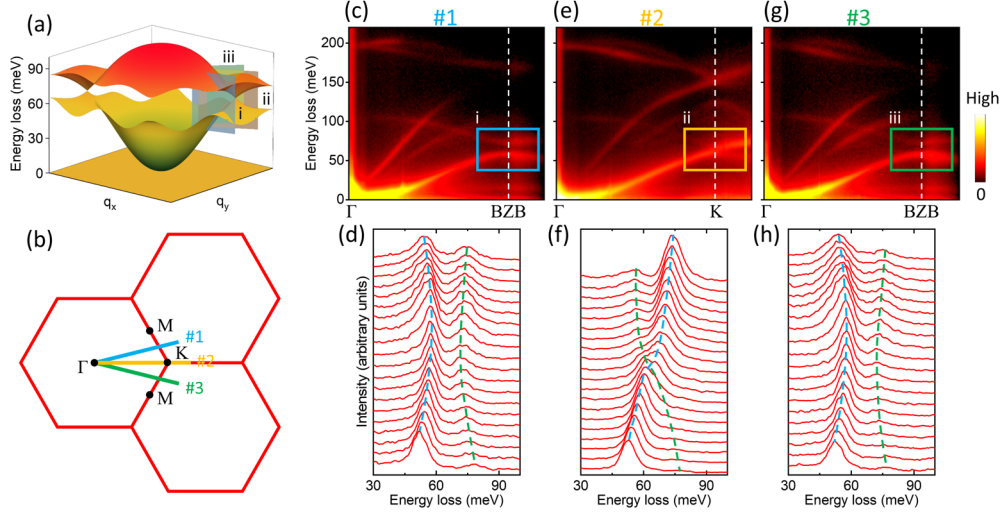


FIG. 4. Dirac phonons of graphene. (a) Demonstration of DP1 from the calculated 3D dispersion plot of the ZA and ZO branches. (b) The schematic of the measurement directions. #2 marks the direction along the Γ -K, #1 and #3 mark the directions $\pm 15^\circ$ off the Γ -K path. (c),(e),(g) The 2D phonon mapping corresponding to the #1, #2, and #3 directions, respectively. The white dotted lines mark the BZ boundary (BZB), and the boxes i, ii, and iii mark the corresponding cuts illustrated in (a). (d),(f),(h) The EDC stacks corresponding to the boxes i, ii, and iii in (c), (e), and (g), respectively.

gap between the LA and ZO modes ($|\omega_{\text{LA}} - \omega_{\text{ZO}}|$) in the first BZ in Figs. 3(b) and 3(d), respectively, revealing that the experimental and calculated contours of the NP1 show the almost identical shape of a rounded hexagon. In similarity, the experimentally measured spectra of both TA and ZO modes [Fig. 3(e)] show good agreement with the calculated ones [Fig. 3(g)], consistently revealing the formation of NP2. Different from NP1, NP2 is highly dispersive with an energy range from ~ 80 to ~ 91 meV in the 3D plot. In the $q_x - q_y$ plane, NP2 exhibits a hexagram-like loop, illustrated by the contour plots of the energy gap between TA and ZO modes ($|\omega_{\text{TA}} - \omega_{\text{ZO}}|$) in the first BZ [Figs. 3(f) and 3(h)].

Note that the NPs of graphene are protected by the M_z symmetry. Breaking the M_z symmetry, which can be achieved by rumpling the two carbon atoms along the out-of-plane direction in the unit cell of graphene, is supposed to open an energy gap in the NPs. Our calculations (Fig. S6 in the SM [25]) indeed show that the NPs open energy gaps, when one of the carbon atoms in the unit cell is rumpled, consolidating the topological origin of the NPs. To date, the largest atomic rumple of graphene has been approximately 0.07 \AA , experimentally achieved on graphene/Ni (111) [43]. But our calculations show that even such a rumple is not big enough to generate an observable gap. The largest NP gap, opened by a 0.07 \AA rumple, is less than 2 meV (Fig. S6 in the SM [25]). This gap is less than the linewidth of the associated phonon branches, and thus is difficult to verify experimentally. It would be possible to realize a larger degree of rumples in some other honeycomb-based structures, such as graphene-functionalized structures [54–56] or emerging 2D materials

(e.g., silicene [57]). The existence of their rumples enables NPs to open larger gaps, which will be promising for undergoing studies.

Identification of Dirac phonons.—Besides the continuous loops of the two NPs, the calculations predict four inequivalent DPs in graphene, as shown in Fig. 2(a). DPs are discrete points at certain positions in the momentum space, forming the conical structures. The type-I DP1, the band crossing between ZA and ZO modes at the K point, is the most obvious one among these DPs. The first-principles calculations demonstrate the DP1 exhibits a conical structure with an energy gap opening in any momentum direction away from the K point [Fig. 4(a)]. To experimentally confirm this conical structure, HREELS measurements along and off the Γ -K path [Fig. 4(b)] were performed. The resulting phononic spectra are displayed in Figs. 4(c), 4(e), and 4(g), along with their corresponding illustrations of the EDC stacks in Figs. 4(d), 4(f), and 4(h) [corresponding to cut i, ii, and iii in Fig. 4(a), respectively]. Apparently, the ZA and ZO modes cross at the K point along the Γ -K direction, while a gap opens along the other directions off the K point. This identifies the conical feature of the type-I DP1. As predicted by the first-principles calculations, the type-I DP2 is formed by the linear band crossing between the LA and LO modes at the K point with the frequency of $\sim 150 \text{ meV}$. At this frequency, our HREELS measurement identifies the existence of the band crossing between the LA and LO modes at the K point [see Fig. 2(c) and SM Fig. S7 [25]] along the Γ -K path. However, along the K -M path our current HREELS technology cannot identify whether the gap between the LA and LO modes exists. This is mainly because the predicted gap between these two modes along the K -M

path [Fig. 2(a)] is even smaller than the allowable highest energy resolution of our measurements. Hence, the conical structure of the type-I DP2 cannot be experimentally verified, although the band crossing between the LA and LO modes along the Γ - K path is clearly observed.

Furthermore, the type-II DP3 and DP4, which originate from the band crossings between the TO and LO modes, have been confirmed by the phononic band crossings along the high-symmetry Γ - M and Γ - K paths, as demonstrated by the experimental EDCs (Fig. S8 in the SM [25]). Unfortunately, it is difficult to currently distinguish whether or not these two branches open a gap away from the crossing points of DP3 and DP4 along the non-high-symmetry paths due to the insufficient energy resolution and the low scattering intensity caused by the selection rule of the HREELS. Nonetheless, the tilted band crossings around DP3 and DP4 are clearly captured by the experimental data, confirming their type-II nature (Fig. S8 in the SM [25]).

In summary, using the HREELS method, we have directly observed the topological NPs and DPs of graphene. These TPs were further predicted to induce topologically protected nontrivial phononic edge states [18], but the current measurement is still challenging (discussed in the SM [25]) for the mapping of these edge states. This will be a direction for future efforts. The HREELS method with 3D phonon mapping highlights a new paradigm for the detection of TPs and lays a foundation for the experimental discovery of widely existing topological bosonic states in crystalline materials.

This work was supported by the National Key R&D Program of China (No. 2021YFA1400200, No. 2021FB3501503, and No. 2022YFA1403000), the National Natural Science Foundation of China (No. 12274446, No. 52021006, No. T2188101, No. 51725103, and No. 52188101), and the Strategic Priority Research Program of the Chinese Academy of Sciences (No. XDB33000000).

J. L., J. L., and J. T. contributed equally to this work.

*hlpeng@pku.edu.cn

†xingqiu.chen@imr.ac.cn

‡jdguo@iphy.ac.cn

§xtzhu@iphy.ac.cn

- [1] F. Li, X. Huang, J. Lu, J. Ma, and Z. Liu, *Nat. Phys.* **14**, 30 (2018).
- [2] H. He, C. Qiu, L. Ye, X. Cai, X. Fan, M. Ke, F. Zhang, and Z. Liu, *Nature (London)* **560**, 61 (2018).
- [3] W. Deng, J. Lu, F. Li, X. Huang, M. Yan, J. Ma, and Z. Liu, *Nat. Commun.* **10**, 1769 (2019).
- [4] X. Huang, W. Deng, F. Li, J. Lu, and Z. Liu, *Phys. Rev. Lett.* **124**, 206802 (2020).
- [5] X. Cai, L. Ye, C. Qiu, M. Xiao, R. Yu, M. Ke, and Z. Liu, *Light* **9**, 38 (2020).
- [6] Y. Yang, J. Lu, M. Yan, X. Huang, W. Deng, and Z. Liu, *Phys. Rev. Lett.* **126**, 156801 (2021).
- [7] H. Miao, T. T. Zhang, L. Wang, D. Meyers, A. H. Said, Y. L. Wang, Y. G. Shi, H. M. Weng, Z. Fang, and M. P. M. Dean, *Phys. Rev. Lett.* **121**, 035302 (2018).
- [8] J. Li, Q. Xie, S. Ullah, R. Li, H. Ma, D. Li, Y. Li, and X.-Q. Chen, *Phys. Rev. B* **97**, 054305 (2018).
- [9] B. W. Xia, R. Wang, Z. J. Chen, Y. J. Zhao, and H. Xu, *Phys. Rev. Lett.* **123**, 065501 (2019).
- [10] Z. J. Chen, R. Wang, B. W. Xia, B. B. Zheng, Y. J. Jin, Y.-J. Zhao, and H. Xu, *Phys. Rev. Lett.* **126**, 185301 (2021).
- [11] J. Li, Q. Xie, J. Liu, R. Li, M. Liu, L. Wang, D. Li, Y. Li, and X.-Q. Chen, *Phys. Rev. B* **101**, 024301 (2020).
- [12] B. Zheng, B. Xia, R. Wang, Z. Chen, J. Zhao, Y. Zhao, and H. Xu, *Phys. Rev. B* **101**, 100303(R) (2020).
- [13] J. Li, J. Liu, S. A. Baronett, M. Liu, L. Wang, R. Li, Y. Chen, D. Li, Q. Zhu, and X.-Q. Chen, *Nat. Commun.* **12**, 1204 (2021).
- [14] X.-Q. Chen, J. Liu, and J. Li, *The Innovation* **2**, 100134 (2021).
- [15] T. T. Zhang, H. Miao, Q. Wang, J. Q. Lin, Y. Cao, G. Fabbris, A. H. Said, X. Liu, H. C. Lei, Z. Fang, H. M. Weng, and M. P. M. Dean, *Phys. Rev. Lett.* **123**, 245302 (2019).
- [16] H. Li, T. Zhang, A. Said, Y. Fu, G. Fabbris, D. G. Mazzone, J. Zhang, J. Lapano, H. N. Lee, H. C. Lei, M. P. M. Dean, S. Murakami, and H. Miao, *Phys. Rev. B* **103**, 184301 (2021).
- [17] Z. Jin, B. Hu, Y. Liu, Y. Li, T. Zhang, K. Iida, K. Kamazawa, A. I. Kolesnikov, M. B. Stone, X. Zhang, H. Chen, Y. Wang, I. A. Zaliznyak, J. M. Tranquada, C. Fang, and Y. Li, *Phys. Rev. B* **106**, 224304 (2022).
- [18] J. Li, L. Wang, J. Liu, R. Li, Z. Zhang, and X.-Q. Chen, *Phys. Rev. B* **101**, 081403(R) (2020).
- [19] Y. Jin, R. Wang, and H. Xu, *Nano Lett.* **18**, 7755 (2018).
- [20] Y. Liu, Y. Xu, S.-C. Zhang, and W. Duan, *Phys. Rev. B* **96**, 064106 (2017).
- [21] X. Zhu, Y. Cao, S. Zhang, X. Jia, Q. Guo, F. Yang, L. Zhu, J. Zhang, E. W. Plummer, and J. Guo, *Rev. Sci. Instrum.* **86**, 083902 (2015).
- [22] H. Ibach, F. C. Bocquet, J. Sforzini, S. Soubatch, and F. S. Tautz, *Rev. Sci. Instrum.* **88**, 033903 (2017).
- [23] A. Al Taleb and D. Farias, *J. Phys. Condens. Matter* **28**, 103005 (2016).
- [24] R. Senga, K. Suenaga, P. Barone, S. Morishita, F. Mauri, and T. Pichler, *Nature (London)* **573**, 247 (2019).
- [25] See Supplemental Material at <http://link.aps.org/supplemental/10.1103/PhysRevLett.131.116602> for details about the sample preparation, experimental and theoretical methods, the substrate effect, and the discussion of topological edge states, including Figs. S1–S8 and Refs. [26–53].
- [26] B. Deng, Z. Pang, S. Chen, X. Li, C. Meng, J. Li, M. Liu, J. Wu, Y. Qi, W. Dang, H. Yang, Y. Zhang, J. Zhang, N. Kang, H. Xu, Q. Fu, X. Qiu, P. Gao, Y. Wei, Z. Liu, and H. Peng, *ACS Nano* **11**, 12337 (2017).
- [27] F. de Juan, A. Politano, G. Chiarello, and H. A. Fertig, *Carbon* **85**, 225 (2015).
- [28] P. R. Wallace, *Phys. Rev.* **71**, 622 (1947).
- [29] A. H. Castro Neto, F. Guinea, N. M. R. Peres, K. S. Novoselov, and A. K. Geim, *Rev. Mod. Phys.* **81**, 109 (2009).
- [30] P. Hohenberg and W. Kohn, *Phys. Rev.* **136**, B864 (1964).
- [31] W. Kohn and L. J. Sham, *Phys. Rev.* **140**, A1133 (1965).

- [32] S. Baroni, S. de Gironcoli, A. Dal Corso, and P. Giannozzi, *Rev. Mod. Phys.* **73**, 515 (2001).
- [33] G. Kresse and J. Hafner, *Phys. Rev. B* **47**, 558 (1993).
- [34] G. Kresse and J. Hafner, *Phys. Rev. B* **49**, 14251 (1994).
- [35] G. Kresse and J. Furthmuller, *Comput. Mater. Sci.* **6**, 15 (1996).
- [36] L. Chaput, A. Togo, I. Tanaka, and G. Hug, *Phys. Rev. B* **84**, 094302 (2011).
- [37] A. Togo and I. Tanaka, *Scr. Mater.* **108**, 1 (2015).
- [38] P. E. Blochl, *Phys. Rev. B* **50**, 17953 (1994).
- [39] G. Kresse and D. Joubert, *Phys. Rev. B* **59**, 1758 (1999).
- [40] J. P. Perdew, K. Burke, and M. Ernzerhof, *Phys. Rev. Lett.* **77**, 3865 (1996).
- [41] M. Vanin, J. J. Mortensen, A. K. Kelkkanen, J. M. Garcia-Lastra, K. S. Thygesen, and K. W. Jacobsen, *Phys. Rev. B* **81**, 081408(R) (2010).
- [42] A. Al Taleb, H. K. Yu, G. Anemone, D. Farías, and A. M. Wodtke, *Carbon* **95**, 731 (2015).
- [43] D. E. Parreiras, E. A. Soares, G. J. P. Abreu, T. E. P. Bueno, W. P. Fernandes, V. E. de Carvalho, S. S. Carara, H. Chacham, and R. Paniago, *Phys. Rev. B* **90**, 155454 (2014).
- [44] L. Zhang and Q. Niu, *Phys. Rev. Lett.* **115**, 115502 (2015).
- [45] Y. Liu, C.-S. Lian, Y. Li, Y. Xu, and W. Duan, *Phys. Rev. Lett.* **119**, 255901 (2017).
- [46] Y. Liu, Y. Xu, and W. Duan, *Research* **2019**, 5173580 (2019).
- [47] B. C. Stipe, M. A. Rezaei, and W. Ho, *Science* **280**, 1732 (1998).
- [48] L. Vitali, M. A. Schneider, K. Kern, L. Wirtz, and A. Rubio, *Phys. Rev. B* **69**, 121414(R) (2004).
- [49] R. Beams, *J. Raman Spectrosc.* **49**, 157 (2018).
- [50] L. Gao, J. R. Guest, and N. P. Guisinger, *Nano Lett.* **10**, 3512 (2010).
- [51] A. C. Ferrari, J. C. Meyer, V. Scardaci, C. Casiraghi, M. Lazzeri, F. Mauri, S. Piscanec, D. Jiang, K. S. Novoselov, S. Roth, and A. K. Geim, *Phys. Rev. Lett.* **97**, 187401 (2006).
- [52] A. Das, S. Pisana, B. Chakraborty, S. Piscanec, S. K. Saha, U. V. Waghmare, K. S. Novoselov, H. R. Krishnamurthy, A. K. Geim, A. C. Ferrari, and A. K. Sood, *Nat. Nanotechnol.* **3**, 210 (2008).
- [53] S. Gottardi, K. Müller, L. Bignardi, J. C. Moreno-López, T. A. Pham, O. Ivashenko, M. Yablonskikh, A. Barinov, J. Björk, P. Rudolf, and M. Stöhr, *Nano Lett.* **15**, 917 (2015).
- [54] J. O. Sofo, A. S. Chaudhari, and G. D. Barber, *Phys. Rev. B* **75**, 153401 (2007).
- [55] H. R. Soni, J. Gebhardt, and A. Görling, *J. Phys. Chem. C* **122**, 2761 (2018).
- [56] D. Lizzit, M. I. Trioni, L. Bignardi, P. Lacovig, S. Lizzit, R. Martinazzo, and R. Larciprete, *ACS Nano* **13**, 1828 (2019).
- [57] M. De Crescenzi, I. Berbezier, M. Scarselli, P. Castrucci, M. Abbarchi, A. Ronda, F. Jardali, J. Park, and H. Vach, *ACS Nano* **10**, 11163 (2016).